Title

CC Chemokine Receptor 5 Targeted Nanoparticles Imaging the Progression and Regression of Atherosclerosis Using Positron Emission Tomography/Computed Tomography

Journal

Molecular Pharmaceutics, 18(3)

ISSN

1543-8384

Authors

Detering, Lisa
Abdilla, Allison
Luehmann, Hannah P
et al.

Publication Date

2021-03-01

DOI

10.1021/acs.molpharmaceut.0c01183

Peer reviewed

Published in final edited form as:

Mol Pharm. 2021 March 01; 18(3): 1386–1396. doi:10.1021/acs.molpharmaceut.0c01183.

CC Chemokine Receptor 5 Targeted Nanoparticles Imaging the Progression and Regression of Atherosclerosis Using Positron Emission Tomography/Computed Tomography

Lisa Detering[1], **Allison Abdilla**[2], **Hannah P. Luehmann**[1], **Jesse W. Williams**[3], **Li-Hao Huang**[3], **Deborah Sultan**[1], **Andrew Elvington**[3], **Gyu Seong Heo**[1], **Pamela K. Woodard**[1], **Robert J. Gropler**[1], **Gwendalyn J. Randolph**[3], **Craig J. Hawker**[2], **Yongjian Liu**[1]

[1]Mallinckrodt Institute of Radiology, Washington University, St. Louis, Missouri 63110, United States.

[2]Materials Department, University of California, Santa Barbara, California 93106, United States.

[3]Department of Pathology and Immunology, Washington University, St. Louis, Missouri 63110, United States.

Abstract

Chemokines and chemokine receptors play an important role in the initiation and progression of atherosclerosis by mediating the trafficking of inflammatory cells. Chemokine receptor 5 (CCR5) has major implications in promoting the development of plaques to advanced stage and related vulnerability. CCR5 antagonist has demonstrated the effective inhibition of atherosclerotic progression in mice, making it a potential biomarker for atherosclerosis management. To accurately determine CCR5 *in vivo*, we synthesized CCR5 targeted Comb nanoparticles through a modular design and construction strategy with control over the physiochemical properties and functionalization of CCR5 targeting peptide D-ala-peptide T-amide (DAPTA-Comb). *In vivo* pharmacokinetic evaluation through ^{64}Cu radiolabeling showed extended blood circulation of ^{64}Cu-DAPTA-Combs conjugated with 10%, 25%, and 40% DAPTA. The different organ distribution profiles of the three nanoparticles demonstrated the effect of DAPTA not only on physicochemical properties, but also targeting efficiency. *In vivo* positron emission tomography/computed tomography (PET/CT) imaging in an apolipoprotein E knock-out mouse atherosclerosis model (ApoE$^{-/-}$) showed that the three ^{64}Cu-DAPTA-Combs could sensitively and specifically detect CCR5 along the progression of atherosclerotic lesions. In an ApoE-encoding adenoviral vector (AAV) induced plaque regression ApoE$^{-/-}$ mouse model, decreased monocyte recruitment,

Corresponding authors: hawker@mrl.ucsb.edu (C.J.H.) and yongjianliu@wustl.edu (Y.L.).

Supporting Information

Synthetic scheme of 10%, 25%, and 40% ^{64}Cu-DAPTA-Combs (S1); Mouse Serum stability of of 40% ^{64}Cu-DAPTA-Comb determined by radio-TLC at 1h, 2h, and 24 h post incubation (S2). Biodistribution of 10%, 25%, and 40% ^{64}Cu-DAPTA-Comb in wild-type C57BL/6 mice (n=4/group) at 1 h, 4 h, and 24 h post-intravenous injection (S3). PET/CT images of 10% ^{64}Cu-DAPTA-Comb in ApoE$^{-/-}$ mice at 8 weeks post HFD at 24 h post injection showing the uptake at aortic arch (S4). Association between 10% ^{64}Cu-DAPTA-Comb uptake in plaques at 16, 28, 35, and 40 weeks post high fat diet and CCR5 RT-PCR data (n=4–5/time point) for aortic arteries of ApoE$^{-/-}$ mice (S5). Summary of PET uptake of 10%, 25%, and 40% ^{64}Cu-DAPTA-Comb in ApoE$^{-/-}$ mice at 8, 16 and 28 weeks post high fat diet (S6).

CONFLICT OF INTEREST

The authors declare no competing financial interest.

CD68+ macrophages, CCR5 expression, and plaque size all associated with reduced PET signals, which not only further confirmed the targeting efficiency of ^{64}Cu-DAPTA-Combs, but also highlighted the potential of these targeted nanoparticles for atherosclerosis imaging. Moreover, the up-regulation of CCR5 and colocalization with CD68+ macrophages in the necrotic core of *ex vivo* human plaque specimens warrants further investigation for atherosclerosis prognosis.

Graphical Abstract

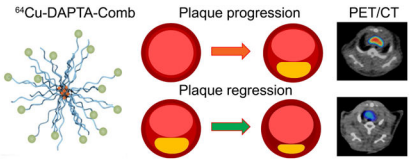

Keywords

nanoparticle; CCR5; atherosclerosis; positron emission tomography; macrophage

INTRODUCTION

Atherosclerosis, the underlying cause of the majority of cardiovascular diseases (CVDs), is a chronic, systemic, primarily-lipid driven inflammatory disease characterized by the development of multifocal plaque lesions within vessel walls, which extend into the vascular lumen.[1, 2] During the progression of atherosclerosis, most atherosclerotic plaques remain asymptomatic, and for many clinical events, the first patient manifestation is stroke, myocardial infarction, or sudden cardiac death. The identification and detection of biomarkers closely associated with the progression or stability of advanced plaques would therefore provide invaluable information about the staging and vulnerability of disease, allowing for personalized therapy and monitoring of treatment response.[3–8]

Of the biomarkers studied in atherosclerosis, most have centered on addressing leukocyte influx in plaque initiation. This establishes a prime role for selectin family members in the capture, tethering, and rolling of circulating monocytes onto the inflamed endothelium, and for endothelial adhesion molecules, which mediate leukocyte arrest by interacting with integrins on activated monocytes.[9–11] However, leukocyte influx in advanced plaque structures have shown large variability during the progression of atherosclerosis, which significantly affects the expression of associated biomarkers and requires further investigation to correlate expression with disease maturation.[6, 12, 13] Chemokines and their receptors are widely expressed and prominently presented on cells that play a crucial role in atherosclerosis development, such as monocytes and macrophages.[14–21] Of the various chemokine/chemokine receptor pairs identified in atherosclerotic plaque, the CCL5/CCR5 axis is one of the most studied systems.[22, 23] In an attempt to find the temporal expression of CCR5 during the progression of atherosclerosis, it was observed that CCR5 showed age-associated increase and played a central role in promoting late-stage plaque.[24] In CCR5 deleted apolipoprotein E (ApoE$^{-/-}$) mice fed with a high fat diet (HFD), the content of monocytes/macrophages and T-lymphocytes in the aorta region was substantially reduced

compared to ApoE$^{-/-}$ mice. As a result, the atherosclerotic plaque was significantly reduced in size and showed improvement toward a less inflammatory phenotype, as evident by reduced T cell/monocyte infiltration and higher smooth muscle and IL-10 content.[25] With CCR5 antagonist Maraviroc treatment in ApoE$^{-/-}$ mice, the plaque size was decreased by 70%, and the monocyte/macrophage infiltration was attenuated by 50%[26], in part because both monocyte subsets in the blood utilize CCR5 in trafficking to plaques.[23] In humans, CCR5 up-regulation in advanced plaque structures was identified and closely associated with plaque stability, demonstrating a significant role for CCR5 as a predictor of atherosclerosis diagnosis and treatment.[27–29]

In atherosclerosis imaging, due to the low abundance of biomarkers expressed on the lesion, the sensitivity and specificity of the imaging probe is essential for successful plaque diagnosis, which makes positron emission tomography (PET) a desirable imaging modality.[6–8] In contrast to monovalent imaging agents, multivalent nanoparticles have demonstrated superior performance based on tunable, high molecular weight structures, which promote targeting efficiency and favorable *in vivo* pharmacokinetics.[30, 31] Core-shell amphiphilic comb copolymers are modular nanostructure designs, which provide for accurate control over functional groups for targeting and imaging, size, charge, and hydrophilicity for minimal non-specific retention. These systems have been studied for the detection of atherosclerotic plaques across various systems, from preclinical research to human translation.[32–36] Of various CCR5 targeting molecules,[37] the DAPTA peptide was chosen due to its CCR5 binding specificity and straightforward conjugation strategy to nanoparticles. Previously, we have reported a DAPTA-Comb nanoparticle conjugated with 10% DAPTA for imaging CCR5 in a mouse vascular injury model.[35] Given the success of on-going clinical study using a natriuretic peptide clearance receptor targeted Comb nanoparticle for human atherosclerosis PET imaging,[36] we aim to further improve the targeting efficiency of DAPTA-Comb for potential translation. We synthesized DAPTA-Comb nanoparticles conjugated with various amounts of DAPTA peptides and assessed the relationship between biodistribution and plaque imaging efficiency. Due to the extended blood retention of DAPTA-Comb, we chose ^{64}Cu as radiolabel owning to its appropriate nuclear properties such as decay half-life ($t_{1/2}$= 12.7 h). We thoroughly assessed ^{64}Cu radiolabeled DAPTA-Combs (^{64}Cu-DAPTA-Combs) plaque imaging sensitivity and specificity in progressive and regressive ApoE$^{-/-}$ mouse atherosclerosis models using PET/CT and correlated the expression of CCR5 on plaques with PET signals. To further assess the potential of CCR5 as an imaging biomarker for human atherosclerosis management, we examined the up-regulation of CCR5 and related histopathological features of *ex vivo* human atherosclerotic specimens collected from carotid endarterectomy (CEA).

MATERIALS AND METHODS

Reagents and instrumentation.

All reagents were used as received unless otherwise specified. 2,5-Dioxopyrrolidin-1-yl pent-4-ynoate was purchased from Annova Chemical Inc. Poly(ethylene glycol)-N_3 (PEG-N_3) was purchased from Nanocs Inc.. Functionalized poly(ethyleneglycol) (PEG) derivatives were purchased from Intezyne Technologies. 1,4,7,10-tetraazacyclododecane-1,4,7-tris(t-

butyl acetate) (DOTA-*t*-Bu-ester), tris-t-butylester-DOTA, 1,4,7,10-tetraazacyclododecane, and DOTA-N-hydroxysuccinimide ester were obtained from Macrocyclics. Amicon Centriplus YM-30 centrifugal filtrations tubes were obtained from Millipore. ^{64}Cu was produced at the Washington University cyclotron facility. D-Ala1-peptide T-amide (DAPTA, D-A1STTTNYT-NH2) was synthesized by CPC Scientific. Zeba desalting spin columns were from Pierce. Polymeric materials were characterized by 1H and 13C nuclear MR (NMR) spectroscopy using a Bruker 500-MHz spectrometer with the residual solvent signal as an internal reference. Gel permeation chromatography was performed in dimethylformamide on a Waters system equipped with four 5-mm Waters columns (300 × 7.7 mm) connected in series with increasing pore size (102, 103, 104, and 106 A°) and Waters 410 differential refractometer index and 996 photodiode array detectors. The molecular weights of the polymers were calculated relative to linear polymethyl methacrylate (PMMA) or PEG standards. Infrared spectra were measured with a Perkin Elmer Spectrum 100 with a Universal ATR sampling accessory.

Mass spectrometry was carried out using matrix-assisted laser desorption/ionization techniques. Gel permeation chromatography (GPC) was carried out with a Waters Alliance HPLC system pump (2695 Separation Module) and four Visco Gel I-Series columns (7.8 mm × 30 cm, Viscotek). A Waters 2414 differential refractometer was used for analysis using dimethyl formamide (DMF) with 0.1 % LiBr as mobile phase. Chromatographic analyses were performed at room temperature and using poly(methyl methacrylate) (PMMA) as standards. Dynamic light scattering (DLS) was performed on a Wyatt Technology DynaPro NanoStar™ at room temperature to determine the hydrodynamic sized of as-prepared nanoparticles. Data was collected on 0.1 wt% aqueous solutions of nanoparticles filtered through a 0.2 μm filter.

Synthetic Procedures.

The synthesis of *S*-methoxycarbonylphenylmethyl dithiobenzoate reversible addition-fragmentation chain-transfer (RAFT) agent,[38] macro- and small molecule monomers, DOTA methacrylate (DOTA-MA), PEG methacrylate (PEGMA), and DAPTA PEG methacrylate (DAPTA-PEGMA), DAPTA-comb copolymers, and nanoparticles were adopted from previously published work with minor modifications.[32–35, 39]

DAPTA-Acetylene.

Synthesis of DAPTA-Acetylene was conductedt as previously reported with the following modification: 2,5-Dioxopyrrolidin-1-yl pent-4-ynoate was used in the place of 4-pentynoic anhydride. MS (MALDI): calculated (M + Na) 960.5, observed (M + Na) 959.7.

Synthesis of DAPTA Poly(ethylene glycol) Methacrylate (DAPTA-PEGMA).

DAPTA-PEGMA was synthesized as previously reported[35] with minor modification using a 0.01 M aqueous ethylenediaminetetraacetic acid (EDTA) solution containing 0.02 M NaOH (× 4) and Milli-Q water (× 10) to wash the product.

Synthesis of DAPTA-Comb Copolymers.

Synthesis of the comb copolymers was performed as previously reported.[34, 35] Percent DAPTA (%DAPTA) is defined as the feed ratio of DAPTA-PEGMA to the total PEG containing monomers (DAPTA-PEGMA + PEGMA). GPC-DMF (PMMA standards): 10% DAPTA-Comb M_w = 200,000 g mol^{-1} Đ = 1.7; 25% DAPTA-Comb M_w = 300,000 g mol^{-1}, Đ = 2.5; 40% DAPTA-Comb M_w = 358,000 g mol^{-1}, Đ = 2.9.

DOTA Deprotection and Nanoparticle Assembly.

Deprotection of the DOTA groups and particle assembly were performed as previously reported.[35] Briefly, after deprotection of the DOTA groups, the freeze-dried comb copolymers were dissolved in dimethyl sulfoxide (DMSO) (1 wt %) and heated to 50°C until fully dissolved. The solution was cooled to room temperature and an equal volume of Milli-Q water was added all at once while stirring to achieve assembly. By changing the ratios of various co-polymers, the number of targeting moieties could be controlled (Figure S1). To remove DMSO, the solution was transferred to 2 Amicon Centriplus YM-30 (molecular weight cut-off = 30,000 g mol^{-1}) centrifugal filtration tubes and concentrated and re-diluted with Milli-Q water until the DMSO content was less than 0.5 mg / mL by ^{1}H NMR (~5 ×). The resultant particles were characterized by DLS and zeta potential with a Zetasizer nano ZS (ZEN3600, Malvern Instruments) (Table 1): 10% DAPTA-Comb: R_h = 14.8 nm, % dispersity = 13.2, ζ-potential = −6.24 mV; 25% DAPTA-Comb: R_h = 15.2 nm, % dispersity = 11.3, ζ-potential =−10.0 mV; 40% DAPTA-Comb: R_h = 10.9 nm, % dispersity = 11.1, ζ-potential =−14.7 mV; non-targeted Comb: R_h= 20.0 nm, % dispersity = 10.1, ζ-potential = −32.0 mV. All the nanoparticle solutions were re-diluted to 10 mg / mL and stored at −20°C.

ApoE$^{-/-}$ Mouse Spontaneous Atherosclerosis Progression Model.

All animal studies were performed in compliance with guidelines set forth by the National Institutes of Health Office of Laboratory Animal Welfare and approved by the Washington University Institutional Animal Care and Use Committee (IACUC). For the spontaneous atherosclerosis mouse model, 6-week-old male ApoE$^{-/-}$mice were fed a high fat diet (HFD) (Harlan Teklad, 42% fat) for 40 weeks. Age-matched wild type (WT) male C57BL/6 mice on normal chow were used as controls. Each mouse was anesthetized with a standard inhaled-anesthetic protocol (1.5%–2% isoflurane) by induction in a chamber, and maintenance anesthesia was administered *via* a nose cone.

ApoE$^{-/-}$ Mouse Atherosclerosis Regression Model.

ApoE$^{-/-}$ mouse atherosclerosis regression model was carried out in apoE$^{-/-}$ mice following our previous report.[22] Six-week-old male apoE$^{-/-}$ mice were first put on HFD for 9 weeks. ApoE$^{-/-}$ mice were injected i.v. with 1.0×10^{12} plaque-forming units per mouse of adeno-associated virus encoding mouse apoE (AAV-252844, Vector Biolabs) or a control PBS solution in a volume of PBS not exceeding 200 μL. Mouse plasma was collected for the measurement of cholesterol levels at baseline, 1, 2, and 3 weeks after adeno-associated virus injection, as we previously reported.[22] To determine the monocyte recruitment during the plaque regression, classic Ly-6C^{hi} monocytes were labeled *in vivo* by retro-orbital i.v.

injection of 1.0 μm fluoresbrite green fluorescent plain microsphere (Polysciences Inc) diluted 1:4 in sterile PBS at 3 days after i.v. injection of 250 μl clodronate-loaded liposomes (Liposoma BV).

^{64}Cu Radiolabeling of DAPTA-Combs and Comb Nanoparticles.

The radiolabeling of DAPTA-comb and comb nanoparticles was as reported previously.[34, 39] The nanoparticles (5 μg, 5 pmol) were heated with ^{64}Cu (~185 MBq) in 100 μL ammonium acetate buffer (0.1 M, pH 5.5) at 80°C for 1 h. EDTA (5 μL, 10 mM in 50 mM pH 7.4 phosphate buffer) was added to the solution and incubated for another 3 min to remove any non-specifically bound ^{64}Cu from the nanoparticles. Then, the ^{64}Cu radiolabeled nanoparticles were purified using a 2 mL zeba spin desalting column. The radiochemical purity (RCP) of the purified nanoparticles was determined by spotting a 2 μL aliquot of the solution on silica gel impregnated glass microfiber chromatography paper developed in a buffer composed of methanol and 10% ammonium acetate (volume ratio = 1:1) and measured by radioactive thin layer chromatography (Radio-TLC, Washington, DC). Repeated procedures would be performed to ensure the RCP equal or greater than 95% prior to *in vivo* studies. Mouse serum stability was performed by incubating 3.5 mCi 40% ^{64}Cu-DAPTA-Comb in 100 μL 1× PBS with 100 μL mouse serum at 37°C with gentle shaking (350 rpm) using an Eppendorf thermomixer (Fisher Scientific, Pittsburgh PA). At 0, 2 and 24 h post incubation, an aliquot of sample was taken out for radio-TLC analysis to determine radiochemical purity.

Biodistribution Studies.

Purified ^{64}Cu-DAPTA-Comb nanoparticles were reconstituted in 0.9% sodium chloride (APP Pharmaceuticals) for intravenous injection. Male C57BL/6 mice weighing 20–25 g (n = 4/group) were anesthetized with inhaled isoflurane, and approximately 370 kBq of labeled nanoparticle s (7.2–9.0 mg/kg of body weight) in 100 μL of saline were injected *via* the tail vein. The mice were reanesthetized before they were euthanized by cervical dislocation at each time point (1, 4, and 24 h) after injection. Organs of interest were collected, weighed, and counted in a well gamma counter (Beckman 8000). Standards were prepared and measured along with the samples to calculate the percentage injected dose per gram of tissue (%ID/gram).[35, 39]

Small-Animal PET/CT Imaging.

Small-animal PET/CT imaging with 10%, 25%, and 40% ^{64}Cu-DAPTA-Comb was performed with ApoE$^{-/-}$ mice on HFD to determine the uptake at the aortic arch along the progression and regression of atherosclerotic lesions. The wild type C57BL/6 mice were used as controls and scanned following the same protocol. For PET/CT imaging with ^{64}Cu-DAPTA-Combs and ^{64}Cu-Comb, 3.7 MBq purified nanoparticles in 100 μL of saline were injected *via* tail vein. The imaging sessions were collected on the PET scanners at 24 h after injection using Inveon PET/CT scanner (Siemens Healthcare). Competitive receptor blocking studies were performed on ApoE$^{-/-}$ mice for ^{64}Cu-DAPTA-Combs by co-injection of unlabeled DAPTA-Comb in 100-fold excess (n=4) at 36 weeks after HFD, followed by PET scans at 24 h post injection. Data analysis of the PET images was performed using the

manufacturer's software (IRW, Siemens Healthcare). The accumulation of the PET tracers at aortic arch was calculated as %ID/gram.

Histology and Immunofluorescence of ApoE$^{-/-}$ Mouse Tissues.

After the last scan, the mice were euthanized by cervical dislocation, and the hearts and aortic arches were either perfusion-fixed in situ with freshly prepared 4% paraformaldehyde in 1×phosphate-buffered saline for histopathology and immunohistochemistry.

Serial sections of 10 μm in thickness were cut from paraformaldehyde-fixed (24 h), OCT-embedded specimens. Blocking serum was added (10% Donkey serum in PBS-T) for 1 h to prevent non-specific binding. The sections were then incubated overnight at 4°C with primary antibody (anti-CD68, 1:100 in 1% blocking serum; Biorad, Hercules, CA and anti-CCR5, 1:100 in 1% blocking serum, Bioss, Woburn, MA). Sections were washed in PBS, and secondary antibodies were applied for 1 h (donkey anti-rat Cy5, 1:300, and donkey anti-rabbit Cy3, 1:300, both from Jackson Laboratories, West Grove, PA). Sections were washed in PBS, and SMA-FITC conjugate was applied for 1 h at room temperature (1:500, Sigma, Saint Louis, MO). Sections were washed again in PBS and coverslipped with DAPI mounting medium before being imaged with confocal microscopy. H&E was also obtained to analyze morphology of the tissues. Quantification of plaque area and area occupied by a particular stain was calculated with ImageJ software. Beads in plaques were counted manually by fluorescence microscopy.[22]

Histology and Immunostaining of Human Tissues.

Human carotid endarterectomy (CEA) specimens were from Washington University Vascular Surgery Biobank Repository collected under Institutional Review Board. De-identified CEA specimens were placed in sterile saline in the operating room and fixed in 10% formalin overnight, embedded in paraffin, and sectioned at a thickness of 5 μm for histology and immunohistochemistry. Whole specimen histologic evaluations were performed using H&E to examine tissue architecture. Paraffin embedded sections were deparaffinized in xylenes and rehydrated using alcohols and PBS. Tissues were boiled in buffer (pH 6.2 Diva Decloaker, 1×) to retrieve antigen. They were blocked with 10% Donkey serum (EMD Millipore, St. Louis, MO) for 1 h to reduce nonspecific binding. The sections were then incubated with primary antibody (anti-CD68, 1:100 in 1% blocking serum; Biorad, Hercules, CA and anti-CCR5, 1:100 in 1% blocking serum, Bioss, MA) overnight at 4 °C. Secondary antibody was applied (donkey anti-rat Cy5, 1:300, and donkey anti-rabbit Cy3, 1:300, both from Jackson Laboratories, West Grove, PA). Sections were washed again in PBS and coverslipped with DAPI mounting medium before being imaged with a Leica confocal microscope system.

Real-time reverse transcription-polymerase chain reaction (RT-PCR).

RNA isolated from aortic arteries were used for real-time RT-PCR. RNeasy MicroRNA Kits (Qiagen; Germantown, MD) was used to isolate RNA following the manufacturer's instruction. Reverse transcription reactions used 300 ng of total RNA, random hexamer priming, and Superscript II reverse transcriptase (Invitrogen). Taqman assays (Invitrogen) were used to determine CCR5 and glyceraldehyde 3-phosphate dehydrogenase (GAPDH)

with an EcoTM Real-Time PCR System (Illumina, San Diego, CA) in 48-well plates (n=3). PCR cycling conditions were as follows: 50°C for 2 min, 95°C for 21 s, and 60°C for 20 s. GAPDH expression was used as a comparator using ΔΔ Ct calculations.

Autoradiography.

Fixed human CEA specimens (n=10) were deparaffinized in Citrasolv and rehydrated with a series of graded alcohols and then PBS. The slides were incubated with 40% ^{64}Cu-DAPTA-Comb (0.75 MBq) for 15 min, followed by extensive wash with water. The slides were then covered with a phosphor-imaging film plate and exposed at −20 °C overnight. The film was imaged with a GE Typhoon FLA 9500 biomolecular imager. For blocking studies, similar procedures were performed in the presence of non-radiolabeled DAPTA-Comb in excess amount (DAPTA-Comb: ^{64}Cu-DAPTA-Comb molar ratio=100:1).

Statistical Analysis.

Group variation is described as mean ± SD. Groups were compared using 1-way ANOVA with a Bonferroni adjustment. Individual group differences were determined using a 2-tailed Mann–Whitney test. The significance level in all tests was a P value of 0.05 or less.

RESULTS AND DISCUSSION

In vivo Pharmacokinetic Evaluation of DAPTA-Combs

In contrast to other nanostructure agents reported for atherosclerosis imaging,[31, 40–42] core-shell comb copolymer systems afford the design flexibility for strategically modifying the nanostructure size, morphology, composition, and surface properties through modular chemistry. This allows nanoparticle candidates to be screened for specific biomedical applications and future translation.[34] Based on our previous work imaging CCR5 in an ApoE$^{-/-}$ mouse vascular injury model[35] using 10% DAPTA-Comb (14 DAPTA peptides/Comb) radiolabeled with ^{64}Cu (^{64}Cu-DAPTA-Comb), we prepared 25% and 40% DAPTA-Comb with ~35 and ~56 DAPTA peptide units per comb nanostructure, respectively following the modular construction strategies (Figure S1, Table 1), to compare and optimize the plaque imaging sensitivity and specificity. Representative mouse serum stability of 40% ^{64}Cu-DAPTA-Comb showed more than 80% intact tracer at 24 h post incubation (Figure S2), ensuring stable radiolabel for CCR5 imaging.

In contrast to previously reported CCR5 peptide targeting tracer ^{64}Cu-DOTA-DAPTA showing fast blood and renal clearance,[35] biodistribution of the three ^{64}Cu-DAPTA-Combs all showed largely extended blood retention, allowing enhanced targeting efficiency.[33–35] At 1 h post injection (p.i.) in wild type (WT) mice, the three ^{64}Cu-DAPTA-Combs showed comparable blood retention (10%: 33.6 ± 7.0 %ID/gram; 25%: 32.4 ± 6.7 %ID/gram; 40%: 27.2 ± 1.2 %ID/gram, n=4). At 4 h p.i., the blood retention of 25% and 40% ^{64}Cu-DAPTA-Comb decreased more than 40% from the value at 1 h, while the 10% counterpart was reduced by approximately 15%. At 24 h p.i., the blood retention of the 10% ^{64}Cu-DAPTA-Comb (21.8 ± 4.2%ID/gram) was almost nine times (9×) higher than those of 25% and 40% ^{64}Cu-DAPTA-Comb (2.3± 0.2 %ID/gram for both). This trend was also observed in other blood pool organs including heart, lung, and muscle (Figures 1 and S3). In the liver, the

10% ^{64}Cu-DAPTA-Comb had relatively stable accumulation during the 24 h study (5.2 ± 1.1 ~ 7.0 ± 0.6%ID/gram), while the 25% and 40% counterparts showed gradually increased uptake with approximately 2, 4, and 5-fold higher accumulations than the values for 10% ^{64}Cu-DAPTA-Comb at 1 h, 4 h, and 24 h. Compared to the progressively increased splenic uptake (3.1± 0.6 ~ 6.9 ± 0.7 %ID/gram) of 10% ^{64}Cu-DAPTA-Comb, the uptake of the corresponding 25% and 40% derivatives in the spleen rapidly increased from 1 h to 4 h. In both cases, the values were ~20 times (20×) higher than for the 10% ^{64}Cu-DAPTA-Comb and remained stable up to 24 h. This trend was likely due to the increased concentration of DAPTA peptide units conjugated to the surface of comb nanoparticle, leading to increased binding to the high levels of CCR5+ immune cells in spleen.[43] In the gastrointestinal tract, 25% and 40% ^{64}Cu-DAPTA-Comb showed slightly higher intestine accumulation at 4 h, but at least doubled uptake at 24 h compared to the 10% counterpart, reasonably due to the hepatobiliary clearance. During the 24 h study, the renal clearance of all three nanoparticles remained constant, albeit the excretion of 40% ^{64}Cu-DAPTA-Comb was slightly higher than the other two (Figure 1).

PET/CT Imaging CCR5 along the Progression of Atherosclerosis Using ^{64}Cu-DAPTA-Comb in an ApoE$^{-/-}$ Mouse Model

PET/CT imaging of CCR5 expression on atherosclerotic lesions was first performed in ApoE$^{-/-}$ mice fed with HFD using 10% ^{64}Cu-DAPTA-Comb along the progression of plaque. As shown in Figure S4, at 8 weeks post HFD, PET/CT images revealed strong uptake at aortic arch of ApoE$^{-/-}$ mouse with little retention observed in the heart, reasonably due to elevated clearance through liver and spleen. At 35 weeks post HFD in ApoE$^{-/-}$ mice, the CCR5 targeted nanoparticles continued to determine an intense PET signal at 24 h post injection in the aortic arch (Figure 2). Quantitative uptake analysis showed that the tracer uptake (7.06 ± 0.46 %ID/g, n=4) was approximately 3 times as much as that determined from WT mice (2.39 ± 0.49 %ID/g, n=4, $p<0.0001$), which showed a weak signal in the aortic arch. Longitudinal PET/CT studies in ApoE$^{-/-}$ mice showed gradually increased uptake at aortic arch from 8 weeks (6.19 ± 0.24%ID/g, n=10) to 28 weeks (7.39 ± 1.15 %ID/g, n=6) post HFD followed by a slow decrease to 6.78 ± 0.65 %ID/g at 40 weeks. In WT mice, due to the lack of atherosclerotic plaque, tracer accumulation at aortic arches was significantly lower than ApoE$^{-/-}$ mice at each time point and hardly changed during the 40 weeks' study (2.07 ± 0.3 %ID/g - 2.55 ± 0.41 %ID/g, $p<0.0001$, n=4–5/group).

The CCR5 targeting specificity of 10% ^{64}Cu-DAPTA-Comb was confirmed through competitive receptor blocking in ApoE$^{-/-}$ mice. In the presence of excess non-radioactive DAPTA-Comb, accumulation of 10% ^{64}Cu-DAPTA-Comb was reduced by more than 50% (3.31 ± 0.71 %ID/g, n=4, $p<0.0001$) at 36 weeks post HFD compared to the signal acquired one week prior in the same group of mice, suggesting targeting specificity. To determine the CCR5 targeting positivity on plaques, the non-specific retention of nanoparticles at atherosclerotic lesions was assessed with non-targeted ^{64}Cu-Comb nanoparticle. As shown in Figure 2, low uptake was demonstrated in ApoE$^{-/-}$ mice. Quantification showed the tracer accumulations (2.09 ± 0.66 %ID/g - 2.69 ± 0.98 %ID/g, n=4 for all, $p<0.0001$ for all) were approximately 2 times less than the results obtained with the targeted 10% ^{64}Cu-DAPTA-Comb at each time point despite the significant progression of atherosclerosis, confirming

the targeting specificity of 10% ^{64}Cu-DAPTA-Comb. Interestingly, with the progression of plaque and decreased cellularity, the CCR5 targeting positivity of 10% ^{64}Cu-DAPTA-Comb gradually increased from 61% at 8 weeks to 70% at 40 weeks post HFD, which could be partially due to the elevated expression of CCR5 on late-stage plaques and reduced non-specific retention,[24] making the tracer a useful tool to determine plaque stability. Moreover, quantitative RT-PCR measurement of CCR5 in aortic arteries of ApoE$^{-/-}$ mice at multiple time points revealed a close association with corresponding tracer uptake of 10% ^{64}Cu-DAPTA-Comb at aortic arch (Figure S5), which further confirmed the imaging specificity of this targeted nanoparticle.

Histopathological analysis of the aortic sinus of ApoE$^{-/-}$ mice at 12 weeks post HFD revealed significant development of atherosclerotic lesions characterized by substantial neointima thickening, large lipid pool, extensive infiltration of foam cells and a thin fibrous cap (Figure 2C). Immunofluorescent staining showed dense expression of CD68 macrophages throughout the plaques. Interestingly, CCR5 signals were mostly determined on the surface of plaque and largely co-localized with CD68 as illustrated in the magnified image (Figure 2C), further supporting the PET imaging data.

Based on biodistribution studies of the three nanoparticles and the PET/CT time-course study with 10% ^{64}Cu-DAPTA-Comb, we further explored the potential of CCR5 imaging using 25% and 40% ^{64}Cu-DAPTA-Combs to gain insight on the effect of DAPTA peptide conjugation on plaque targeting efficiency along the progression of atherosclerosis in ApoE$^{-/-}$ mice fed on HFD for 8, 16, and 28 weeks. As shown in Figure 3A, 25% ^{64}Cu-DAPTA-Comb nanoparticles showed a strong PET signal within the aortic arch of ApoE$^{-/-}$ mice at 28 weeks post HFD in contrast to weak accumulation in WT mice. Quantitative uptake analysis revealed a gradually increased uptake at plaques in ApoE$^{-/-}$ mice and progressively declining accumulation in WT mice during the time-course study, similar to what was determined using 10% ^{64}Cu-DAPTA-Comb. In contrast to the data acquired with 10% ^{64}Cu-DAPTA-Comb (~14 DAPTA/Comb), the 25% ^{64}Cu-DAPTA-Comb (~35 DAPTA/Comb) demonstrated approximately 20% higher uptake in plaques during the time-course study ($p<0.01$ at both 8 and 28 weeks, n=4–8/group) (Figure S6). Importantly, 25% ^{64}Cu-DAPTA-Comb plaque uptake at 28 weeks (9.05±0.67%ID/g, n=4) was significantly higher than those at 8 weeks (7.53±0.31%ID/g, n=8, $p<0.0001$) and 16 weeks (8.02±0.38%ID/g, n=4, $p<0.05$), suggesting its sensitivity to monitor the progression of plaque. ApoE$^{-/-}$/WT tracer uptake ratios at the three time points for 25% ^{64}Cu-DAPTA-Comb (3.8, 4.0, 5.1 for 8, 16, and 28 weeks, respectively) were all higher than those obtained with 10% counterpart (2.5, 2.9, 3.0) at the same time points, indicating DAPTA peptide mediated tracer uptake at atherosclerotic lesions (Figure 3B). Evaluation of the 40% ^{64}Cu-DAPTA-Comb demonstrated significantly increased uptake (approximately 25% higher, $p<0.01$, $p<0.05$, and $p<0.001$ at 8, 16 and 28 weeks, respectively, n=4–8/group) and uptake ratios (3.8, 4.9, 5.6) at each time point relative to those obtained with 10% ^{64}Cu-DAPTA-Comb (Figure S6). Furthermore, 40% ^{64}Cu-DAPTA-Comb uptake at 16 weeks (8.80±0.63%ID/g, n=4, $p<0.05$) and 28 weeks (9.47±0.72%ID/g, n=4, $p<0.005$) was both significantly higher than those acquired at 8 weeks (7.61±0.55, n=8). Importantly, competitive receptor blocking at 28 weeks demonstrated more than 67% decreased uptake (3.10±0.47, n=4, $p<0.0001$), confirming the plaque targeting specificity of 40% ^{64}Cu-DAPTA-Comb. This is again in

agreement with the conjugation of more DAPTA peptide units (~56 DAPTA/Comb) leading to more efficient CCR5 targeting (Figure 3C, D). These results are also consistent with the above biodistribution study and our previous report demonstrating the importance of nanoparticle's structure and functionalization for optimal targeting of atherosclerosis.[34]

PET/CT Imaging the Monocytes Recruitment Dynamics in Regressive Atherosclerosis

The development of atherosclerosis involves recruitment of monocytes from blood to plaques and local proliferation of macrophages[1, 44], which leads to dynamic variation of chemokine receptor concentrations. The sensitivity of an imaging agent for the detection of these dynamic changes is important for tracking the progression and regression of atherosclerosis to optimize treatment. Previously, we characterized plaque regression by treating ApoE$^{-/-}$ mice with ApoE-encoding adenoviral vector (AAV), showing significant decrease of cholesterol, considerable decrease of CD68+ macrophages at plaques, and effective reduction of plaque size.[22] To determine and compare the sensitivity of the three ^{64}Cu-DAPTA-Combs tracking plaque regression, we performed AAV treatment in 9-week-old ApoE$^{-/-}$ mice and imaged the mice at 3 weeks post treatment along with non-treated ApoE$^{-/-}$ mice on HFD. As shown in Figure 4A, plasma cholesterol levels in the AAV treated ApoE$^{-/-}$ mice (AAV group) were significantly decreased at 1 week post treatment and throughout the 3 weeks' study compared to the mice without treatment (No AAV group), which was consistent with our previous data.[22] PET/CT images with three ^{64}Cu-DAPTA-Combs all revealed intensive tracer accumulations at aortic arches in no AAV mice compared to the decreased uptake in the AAV group. Quantitative uptake analysis showed 45.8 ± 5.6 %, 52.8 ± 8.3% and 63 ± 6.4% decrease in AAV treated mice compared to the no AAV group ($p<0.0001$ for all, n=4–5/group) for the 10%, 25%, and 40% ^{64}Cu-DAPTA-Comb, respectively (Figure 4B). The tracer uptake difference between the AAV and no AAV groups from 10% to 40% ^{64}Cu-DAPTA-Combs was consistent with the results abovementioned in the progressive plaques, suggesting increased sensitivity of 40% ^{64}Cu-DAPTA-Comb in detecting atherosclerosis (Figure 4C).

Histopathological characterization of the impact of AAV treatment revealed decreased lipid pool, reduced infiltration of foam cells, and less neointimal thickening in the aortic sinus of AAV treated mice relative to the untreated group (Figure 4D). Immunofluorescent staining of the aortic sinus also showed reduced CD68+ macrophages and CCR5 signals in AAV treated mice compared to the ApoE$^{-/-}$ mice without AAV treatment. As we previously reported, through the transient depletion of monocytes using clodronate-loaded liposome followed by the introduction of fluorescent latex beads, the recruitment of proinflammatory monocytes from bone marrow to plaque can be determined by tracking these fluorescent beads.[23] As shown in Figure 4E, the fluorescence signals showed approximately 3-fold less latex+ cells in the AAV treated group compared to the untreated group, confirming decreased monocyte recruitment to plaques. Quantification of the atherosclerotic lesions demonstrated decreased plaque size from 0.46 ± 0.08 μm^2 in the no AAV group to 0.22 ± 0.08 μm^2 in AAV treated mice (Figure 4F), which was consistent with reduced monocyte recruitment. These characterizations strongly supported the PET imaging sensitivity and specificity of CCR5 targeted ^{64}Cu-DAPTA-Combs to determine plaque regression following AAV treatment in ApoE$^{-/-}$ mice.

Assessment of CCR5 Expression in Human Carotid Endarterectomy (CEA) Specimens

Though the expression of CCR5 has been reported in human atherosclerotic tissues,[45] we examined the level of CCR5 in human CEA specimens to further assess its potential as a biomarker for plaque imaging and therapy.[33, 46] As shown in Figure 5, histological analysis of representative CEA tissue showed significant neointimal thickening, a large lipid-rich necrotic core (NC), high infiltration of foam cells, and some regions with a thin fibrous cap, suggesting a vulnerable phenotype.[47, 48] Immunofluorescent staining revealed dense expression of CD68+ macrophages throughout the tissue, with most signals residing in the necrotic core. CCR5 staining showed high expression in the NC region, largely co-localized with CD68 (Figure 5E, F), suggesting its potential for further investigation in human atherosclerosis. *Ex vivo* autoradiography using 40% ^{64}Cu-DAPTA-Comb revealed significant binding to human CEA in a similar profile to CCR5 immunostaining, suggesting its binding specificity (Figure 5G). Competitive autoradiography blocking using non-radioactive 40% DAPTA-Comb showed largely reduced signal in CEA specimen (Figure 5H), confirming the binding specificity.

CONCLUSIONS

Through the modular design and construction of multi-functional nanostructures, we have synthesized and optimized three CCR5 targeted ^{64}Cu-DAPTA-Comb nanoparticles with accurate control over the physicochemical properties and surface functionalization for atherosclerosis imaging using PET/CT. *In vivo* pharmacokinetic evaluation demonstrated extended blood circulation and a correlation between the level of the conjugated DAPTA peptide units and organ distribution. All three targeting nanoparticles showed sensitive and specific detection of CCR5 in plaques, not only along the progression of atherosclerotic lesions, but also during plaque regression in an ApoE$^{-/-}$ mouse model. In contrast to the 10% and 25% ^{64}Cu-DAPTA-Combs, the 40% ^{64}Cu-DAPTA-Comb revealed superior sensitivity and specificity for imaging of CCR5 up-regulation on atherosclerotic lesions. Biological characterization of AAV treatment effect in ApoE$^{-/-}$ mice and its association with PET signals further confirmed the plaque targeting efficiency of these multi-functional nanoparticles. *Ex vivo* characterization of CCR5 in human CEA specimens highlighted its potential as a prognostic biomarker for atherosclerosis mangement. However, there are some limitations for the current study. Mouse serum stabily study showed significant dissociation of ^{64}Cu from DOTA at 24 h. A more stable chelator such as 5-(8-methyl-3,6,10,13,16,19-hexaaza-bicyclo[6.6.6]icosan-1-ylamino)-5-oxopentanoic acid (MeCOSar) needs to be used to further improve the biodistributin profile and reduce liver uptake.[49] Compared to the acute AAV treatment, future studies are warranted using a more clinically relevant treatment such as statin-based therapy or cessation of HFD in ApoE$^{-/-}$ mice to assess the sensitivity of 40% ^{64}Cu-DAPTA-Comb detecting the subtle variation of the plaques. Moreover, comparing to human plaques, it is known that ApoE$^{-/-}$ model does not rupture, the as-developed nanoprobe may need to be further assessed in ApoE$^{-/-}$Fbn1$^{C1039G+/-}$ mice with vulnerable atherosclerotic lesions that eventually rupture.[50] Results acquired from these studies will promote the translation of as-developed ^{64}Cu-DAPTA-Combs to diagnose high-risk patients for surgical intervention or serve as a companion imaging approach for targeted treatment given the availability of CCR5 antagonists used in clinic.

Supplementary Material

Refer to Web version on PubMed Central for supplementary material.

ACKNOWLEDGMENTS

This work was supported by 1R35HL145212, R00HL138163 from the National Heart, Lung, and Blood Institute of the National Institutes of Health. The characterization of nanoparticles was performed in the Shared Facilities of the National Science Foundation (NSF) Materials Research and Engineering Center at UC Santa Barbara, DMR-1720256. We thank Nicole Fettig, Margaret Morris, Amanda Klaas, and Lori Strong for their assistance with the biodistribution and imaging studies in animals; Alaina McGrath for synthesis help and Thomas Voller, Evelyn Madrid, and Paul Eisenbeis for ^{64}Cu production.

REFERENCES

(1). Tuttolomondo A; Di Raimondo D; Pecoraro R; Arnao V; Pinto A; Licata G Atherosclerosis As an Inflammatory Disease. Curr. Pharm. Des 2012, 18, 4266–4288. [PubMed: 22390643]

(2). Libby P Inflammation in Atherosclerosis. Arterioscler. Thromb. Vasc. Biol 2012, 32, 2045–2051. [PubMed: 22895665]

(3). Wildgruber M; Swirski FK; Zernecke A Molecular Imaging of Inflammation in Atherosclerosis. Theranostics 2013, 3, 865–884. [PubMed: 24312156]

(4). Orbay H; Hong H; Zhang Y; Cai W Positron Emission Tomography Imaging of Atherosclerosis. Theranostics 2013, 3, 894–902. [PubMed: 24312158]

(5). Quillard T; Libby P Molecular Imaging of Atherosclerosis for Improving Diagnostic and Therapeutic Development. Circ. Res 2012, 111, 231–244. [PubMed: 22773426]

(6). Piri R; Gerke O; Hoilund-Carlsen PF Molecular Imaging of Carotid Artery Atherosclerosis with PET: A Systematic Review. Eur. J. Nucl. Med. Mol. Imaging 2020, 47, 2016–2025. [PubMed: 31786626]

(7). Hoilund-Carlsen PF; Moghbel MC; Gerke O; Alavi A Evolving Role of PET in Detecting and Characterizing Atherosclerosis. PET Clin 2019, 14, 197–209. [PubMed: 30826018]

(8). Daghem M; Bing R; Fayad ZA; Dweck MR Noninvasive Imaging to Assess Atherosclerotic Plaque Composition and Disease Activity: Coronary and Carotid Applications. JACC Cardiovasc. Imaging 2020, 13, 1055–1068. [PubMed: 31422147]

(9). Dong ZM; Brown AA; Wagner DD Prominent Role of P-selectin in the Development of Advanced Atherosclerosis in Apoe-deficient Mice. Circulation 2000, 101, 2290–2295. [PubMed: 10811597]

(10). Libby P; DiCarli M; Weissleder R The Vascular Biology of Atherosclerosis and Imaging Targets. J. Nucl. Med 2010, 51 Suppl 1, 33S–37S. [PubMed: 20395349]

(11). Nakashima Y; Raines EW; Plump AS; Breslow JL; Ross R Upregulation of VCAM-1 and ICAM-1 at Atherosclerosis-prone Sites on the Endothelium in the Apoe-deficient Mouse. Arterioscler. Thromb. Vasc. Biol 1998, 18, 842–851. [PubMed: 9598845]

(12). Foss CA; Sanchez-Bautista J; Jain SK Imaging Macrophage-associated Inflammation. Semin. Nucl. Med 2018, 48, 242–245. [PubMed: 29626941]

(13). Miteva K; Madonna R; De Caterina R; Van Linthout S Innate and Adaptive Immunity in Atherosclerosis. Vascul. Pharmacol 2018, 107, 67–77.

(14). John AE; Channon KM; Greaves DR, Chemokines, Chemokine Receptros and Atherosclerosis. In Chemokines, Chemokine Receptors, and Disease, Schwiebert LM, Ed. Elsevier: Amesterdam, The Netherlands, 2005; pp 223–253.

(15). Kraaijeveld AO; de Jager SC; van Berkel TJ; Biessen EA; Jukema JW Chemokines and Atherosclerotic Plaque Progression: Towards Therapeutic Targeting? Curr. Pharm. Des 2007, 13, 1039–1052. [PubMed: 17430167]

(16). Bursill CA; Channon KM; Greaves DR The Role of Chemokines in Atherosclerosis: Recent Evidence from Experimental Models and Population Genetics. Curr. Opin. Lipidol 2004, 15, 145–149. [PubMed: 15017357]

(17). White GE; Iqbal AJ; Greaves DR CC Chemokine Receptors and Chronic Inflammation--Therapeutic Opportunities and Pharmacological Challenges. Pharmacol. Rev 2013, 65, 47–89. [PubMed: 23300131]

(18). Zernecke A; Shagdarsuren E; Weber C Chemokines in Atherosclerosis: An update. Arterioscler. Thromb. Vasc. Biol 2008, 28, 1897–1908. [PubMed: 18566299]

(19). Weber C; Schober A; Zernecke A Chemokines: Key Regulators of Mononuclear Cell Recruitment in Atherosclerotic Vascular Disease. Arterioscler. Thromb. Vasc. Biol 2004, 24, 1997–2008. [PubMed: 15319268]

(20). Liu Y; Woodard PK Chemokine Receptors: Key for Molecular Imaging of Inflammation in Atherosclerosis. J Nucl Cardiol 2019, 26, 1179–1181. [PubMed: 29516368]

(21). Li W; Luehmann HP; Hsiao HM; Tanaka S; Higashikubo R; Gauthier JM; Sultan D; Lavine KJ; Brody SL; Gelman AE; Gropler RJ; Liu Y; Kreisel D Visualization of Monocytic Cells in Regressing Atherosclerotic Plaques by Intravital 2-Photon and Positron Emission Tomography-Based Imaging-Brief Report. Arterioscler. Thromb. Vasc. Biol 2018, 38, 1030–1036. [PubMed: 29567678]

(22). Potteaux S; Gautier EL; Hutchison SB; van Rooijen N; Rader DJ; Thomas MJ; Sorci-Thomas MG; Randolph GJ Suppressed Monocyte Recruitment Drives Macrophage Removal from Atherosclerotic Plaques of Apoe−/− Mice During Disease Regression. J. Clin. Invest 2011, 121, 2025–2036. [PubMed: 21505265]

(23). Tacke F; Alvarez D; Kaplan TJ; Jakubzick C; Spanbroek R; Llodra J; Garin A; Liu J; Mack M; van Rooijen N; Lira SA; Habenicht AJ; Randolph GJ Monocyte Subsets Differentially Employ Ccr2, Ccr5, and Cx3cr1 to Accumulate within Atherosclerotic Plaques. J. Clin. Invest 2007, 117, 185–194. [PubMed: 17200718]

(24). Quinones MP; Martinez HG; Jimenez F; Estrada CA; Dudley M; Willmon O; Kulkarni H; Reddick RL; Fernandes G; Kuziel WA; Ahuja SK; Ahuja SS Cc Chemokine Receptor 5 Influences Late-Stage Atherosclerosis. Atherosclerosis 2007, 195, e92–103. [PubMed: 17466311]

(25). Braunersreuther V; Zernecke A; Arnaud C; Liehn EA; Steffens S; Shagdarsuren E; Bidzhekov K; Burger F; Pelli G; Luckow B; Mach F; Weber C Ccr5 But Not Ccr1 Deficiency Reduces Development of Diet-induced Atherosclerosis in Mice. Arterioscler. Thromb. Vasc. Biol 2007, 27, 373–379. [PubMed: 17138939]

(26). Cipriani S; Francisci D; Mencarelli A; Renga B; Schiaroli E; D'Amore C; Baldelli F; Fiorucci S Efficacy of The Ccr5 Antagonist Maraviroc in Reducing Early, Ritonavir-induced Atherogenesis and Advanced Plaque Progression in Mice. Circulation 2013, 127, 2114–2124. [PubMed: 23633271]

(27). Fernandez-Sender L; Alonso-Villaverde C; Rull A; Rodriguez-Gallego E; Riera-Borrull M; Hernandez-Aguilera A; Camps J; Beltran-Debon R; Aragones G; Menendez JA; Joven J A Possible Role for Ccr5 in the Progression of Atherosclerosis in HIV-infected Patients: A Cross-sectional Study. AIDS Res. Ther 2013, 10, 11. [PubMed: 23659629]

(28). Papaspyridonos M; Smith A; Burnand KG; Taylor P; Padayachee S; Suckling KE; James CH; Greaves DR; Patel L Novel Candidate Genes in Unstable Areas of Human Stherosclerotic Plaques. Arterioscler. Thromb. Vasc. Biol 2006, 26, 1837–1844. [PubMed: 16741146]

(29). Lin CS; Hsieh PS; Hwang LL; Lee YH; Tsai SH; Tu YC; Hung YW; Liu CC; Chuang YP; Liao MT; Chien S; Tsai MC The Ccl5/ccr5 Axis Promotes Vascular Smooth Muscle Cell Proliferation and Atherogenic Phenotype Switching. Cell Physiol. Biochem 2018, 47, 707–720. [PubMed: 29794461]

(30). Bejarano J; Navarro-Marquez M; Morales-Zavala F; Morales JO; Garcia-Carvajal I; Araya-Fuentes E; Flores Y; Verdejo HE; Castro PF; Lavandero S; Kogan MJ Nanoparticles for Diagnosis and Therapy of Atherosclerosis and Myocardial Infarction: Evolution Toward Prospective Theranostic Approaches. Theranostics 2018, 8, 4710–4732. [PubMed: 30279733]

(31). Flores AM; Ye J; Jarr KU; Hosseini-Nassab N; Smith BR; Leeper NJ Nanoparticle Therapy for Vascular Diseases. Arterioscler. Thromb. Vasc. Biol 2019, 39, 635–646. [PubMed: 30786744]

(32). Luehmann HP; Detering L; Fors BP; Pressly ED; Woodard PK; Randolph GJ; Gropler RJ; Hawker CJ; Liu Y Pet/ct Imaging of Chemokine Receptors in Inflammatory Atherosclerosis Using Targeted Nanoparticles. J. Nucl. Med 2016, 57, 1124–1129. [PubMed: 26795285]

(33). Liu Y; Luehmann HP; Detering L; Pressly ED; McGrath AJ; Sultan D; Nguyen A; Grathwohl S; Shokeen M; Zayed M; Gropler RJ; Abendschein D; Hawker CJ; Woodard PK Assessment of Targeted Nanoparticle Assemblies for Atherosclerosis Imaging with Positron Emission Tomography and Potential for Clinical Translation. ACS Appl. Mater. Interfaces 2019, 11, 15316–15321. [PubMed: 30969098]

(34). Woodard PK; Liu Y; Pressly ED; Luehmann HP; Detering L; Sultan DE; Laforest R; McGrath AJ; Gropler RJ; Hawker CJ Design and Modular Construction of A Polymeric Nanoparticle for Targeted Atherosclerosis Positron Emission Tomography Imaging: A Story of 25% (64)Cu-canf-comb. Pharm. Res 2016, 33, 2400–2410. [PubMed: 27286872]

(35). Luehmann HP; Pressly ED; Detering L; Wang C; Pierce R; Woodard PK; Gropler RJ; Hawker CJ; Liu Y PET/CT Imaging of Chemokine Receptor CCR5 in Vascular Injury Model Using Targeted Nanoparticle. J. Nucl. Med 2014, 55, 629–934. [PubMed: 24591489]

(36). PET Imaging of Natriuretic Peptide Receptor C (npr-c) in Carotid Atherosclerosis. https://clinicaltrials.gov/ct2/show/NCT02417688?term=woodard&draw=2&rank=7

(37). Aldinucci D; Borghese C; Casagrande N The Ccl5/ccr5 Axis in Cancer Progression. Cancers (Basel) 2020, 12.

(38). Perrier S; Takolpuckdee P; Westwood J; Lewis DM Versatile Chain Transfer Agents for Reversible Addition Fragmentation Chain Transfer (raft) Polymerization to Synthesize Functional Polymeric Architectures. Macromolecules 2004, 37, 2709–2717.

(39). Pressly ED; Pierce RA; Connal LA; Hawker CJ; Liu Y Nanoparticle PET/CT Imaging of Natriuretic Peptide Clearance Receptor in Prostate Cancer. Bioconjug. Chem 2013, 24, 196–204. [PubMed: 23272904]

(40). Beldman TJ; Malinova TS; Desclos E; Grootemaat AE; Misiak ALS; van der Velden S; van Roomen C; Beckers L; van Veen HA; Krawczyk PM; Hoebe RA; Sluimer JC; Neele AE; de Winther MPJ; van der Wel NN; Lutgens E; Mulder WJM; Huveneers S; Kluza E Nanoparticle-aided Characterization of Arterial Endothelial Architecture during Atherosclerosis Progression and Metabolic Therapy. ACS Nano 2019, 13, 13759–13774. [PubMed: 31268670]

(41). Lariviere M; Lorenzato CS; Adumeau L; Bonnet S; Hemadou A; Jacobin-Valat MJ; Noubhani A; Santarelli X; Minder L; Di Primo C; Sanchez S; Mornet S; Laroche-Traineau J; Clofent-Sanchez G Multimodal Molecular Imaging of Atherosclerosis: Nanoparticles Functionalized with Scfv Fragments of An Anti-Alphaiibbeta3 Antibody. Nanomedicine 2019, 22, 102082. [PubMed: 31404651]

(42). Banik B; Surnar B; Askins B; Banerjee M; Dhar S Dual Targeted Synthetic Nanoparticle for Cardiovascular Diseases. ACS Appl. Mater. Interfaces 2020, 12, 6852–6862. [PubMed: 31886643]

(43). Bronte V; Pittet MJ The Spleen in Local and Systemic Regulation of Immunity. Immunity 2013, 39, 806–818. [PubMed: 24238338]

(44). Robbins CS; Hilgendorf I; Weber GF; Theurl I; Iwamoto Y; Figueiredo JL; Gorbatov R; Sukhova GK; Gerhardt LM; Smyth D; Zavitz CC; Shikatani EA; Parsons M; van Rooijen N; Lin HY; Husain M; Libby P; Nahrendorf M; Weissleder R; Swirski FK Local Proliferation Dominates Lesional Macrophage Accumulation in Atherosclerosis. Nat. Med 2013, 19, 1166–1172. [PubMed: 23933982]

(45). Jones KL; Maguire JJ; Davenport AP Chemokine Receptor Ccr5: From Aids to Atherosclerosis. Br. J. Pharmacol 2011, 162, 1453–1469. [PubMed: 21133894]

(46). Heo GS; Kopecky B; Sultan D; Ou M; Feng G; Bajpai G; Zhang X; Luehmann H; Detering L; Su Y; Leuschner F; Combadière C; Kreisel D; Gropler RJ; Brody SL; Liu Y; Lavine KJ Molecular Imaging Visualizes Recruitment of Inflammatory Monocytes and Macrophages to the Injured Heart. Circ. Res 2019, 124, 881–890. [PubMed: 30661445]

(47). van Lammeren GW; Moll FL; Borst GJ; de Kleijn DP; de Vries JP PM; Pasterkamp G Atherosclerotic Plaque Biomarkers: Beyond the Horizon of the Vulnerable Plaque. Curr. Cardiol. Rev 2011, 7, 22–27. [PubMed: 22294971]

(48). Koenig W; Khuseyinova N Biomarkers of Atherosclerotic Plaque Instability and Rupture. Arterioscler. Thromb. Vasc. Biol 2007, 27, 15–26. [PubMed: 17082488]

(49). Keinänen O; Fung K; Brennan JM; Zia N; Harris M; van Dam E; Biggin C; Hedt A; Stoner J; Donnelly PS; Lewis JS; Zeglis BM Harnessing 64 Cu/ 67 Cu for a theranostic approach to pretargeted radioimmunotherapy. Proc. Natl. Acad. Sci. U S A 2020, 117, 28316–28327. [PubMed: 33106429]

(50). von Scheidt M; Zhao Y; Kurt Z; Pan C; Zeng L; Yang X; Schunkert H; Lusis AJ Applications and Limitations of Mouse Models for Understanding Human Atherosclerosis. Cell Metab 2017, 25, 248–261. [PubMed: 27916529]

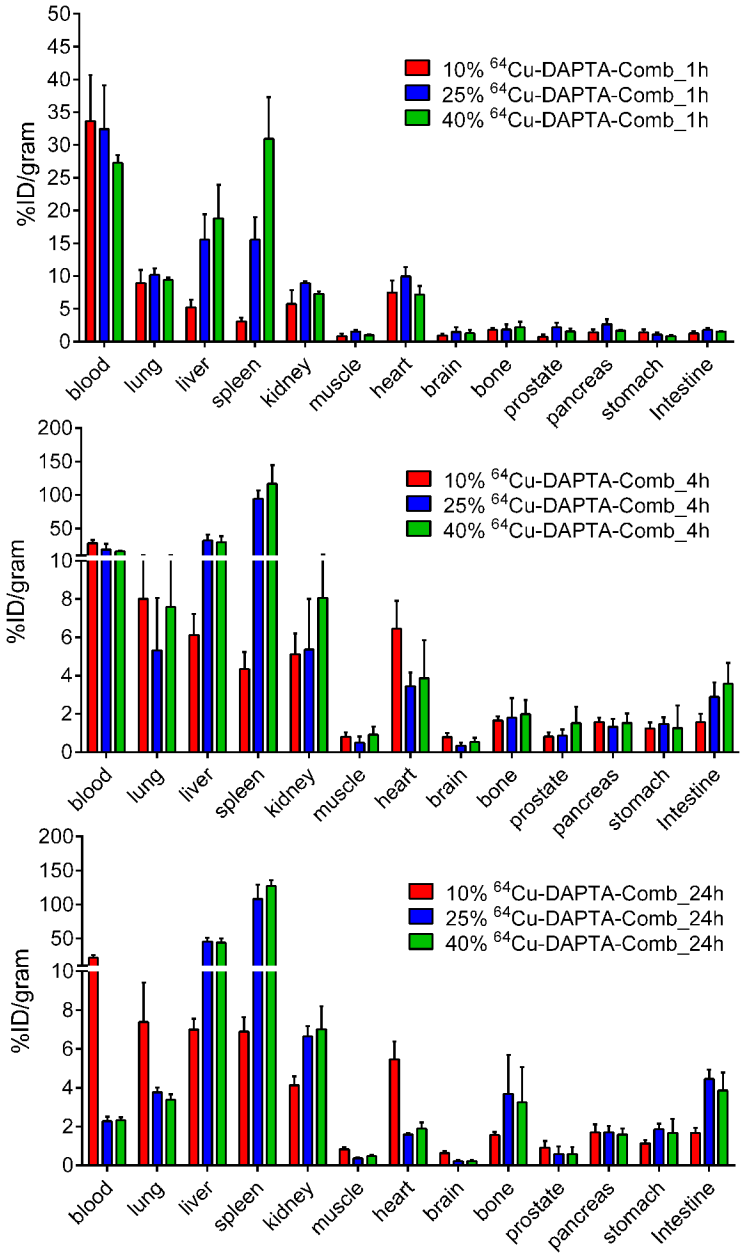

Figure 1.

Biodistribution of 10%, 25%, and 40% ^{64}Cu-DAPTA-Comb in wild-type C57BL/6 mice (n=4/group) at (A) 1 h, (B) 4 h, and (C) 24 h post-intravenous injection. **** p<0.0001, *** p<0.001, ** p<0.01, * p<0.05.

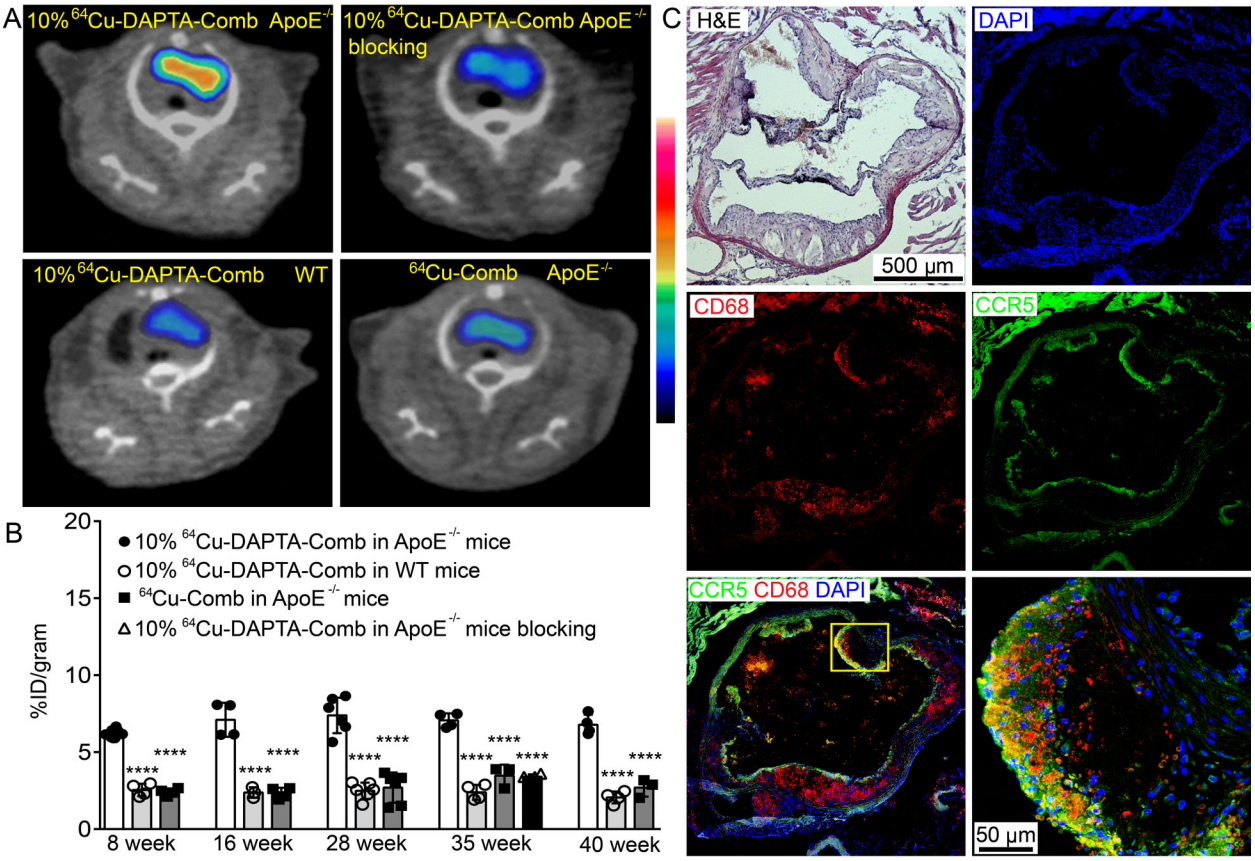

Figure 2.

(A) Representative 10% ^{64}Cu-DAPTA-Comb PET/CT images at 24 h post injection showing specific targeting at aortic arch in ApoE$^{-/-}$ mice, significantly blocked signal with the co-injection of non-radiolabeled DAPTA-Comb, and minimum uptake in wild-type C57BL/6 mice. Non-targeted ^{64}Cu-Comb image showed low, non-specific uptake at aortic arch. All the studies were performed in ApoE$^{-/-}$ mice at 35 weeks post HFD and WT mice on normal chow. (B) Quantitative uptake analysis of 10% ^{64}Cu-DAPTA-Comb in ApoE$^{-/-}$ and age-matched wild-type C57BL/6 mice and non-targeted ^{64}Cu-Comb in ApoE$^{-/-}$ mice in a time course study. Competitive receptor blocking study was performed in ApoE$^{-/-}$ mice (**** $p<0.0001$, n=4–6/group). (C) H&E staining of aortic sinus of ApoE$^{-/-}$ mice on HFD for 12 weeks showing the development of atherosclerotic lesion with significant neointimal thickening, large lipid pool, and infiltration of foam cells. Immunofluorescent staining showing DAPI (blue), CD68 macrophage (red), CCR5 (green) and fused images. CD68 expression was largely throughout the plaques, while CCR5 was more on the surface of plaques and co-localized with CD68 (amplified image, yellow).

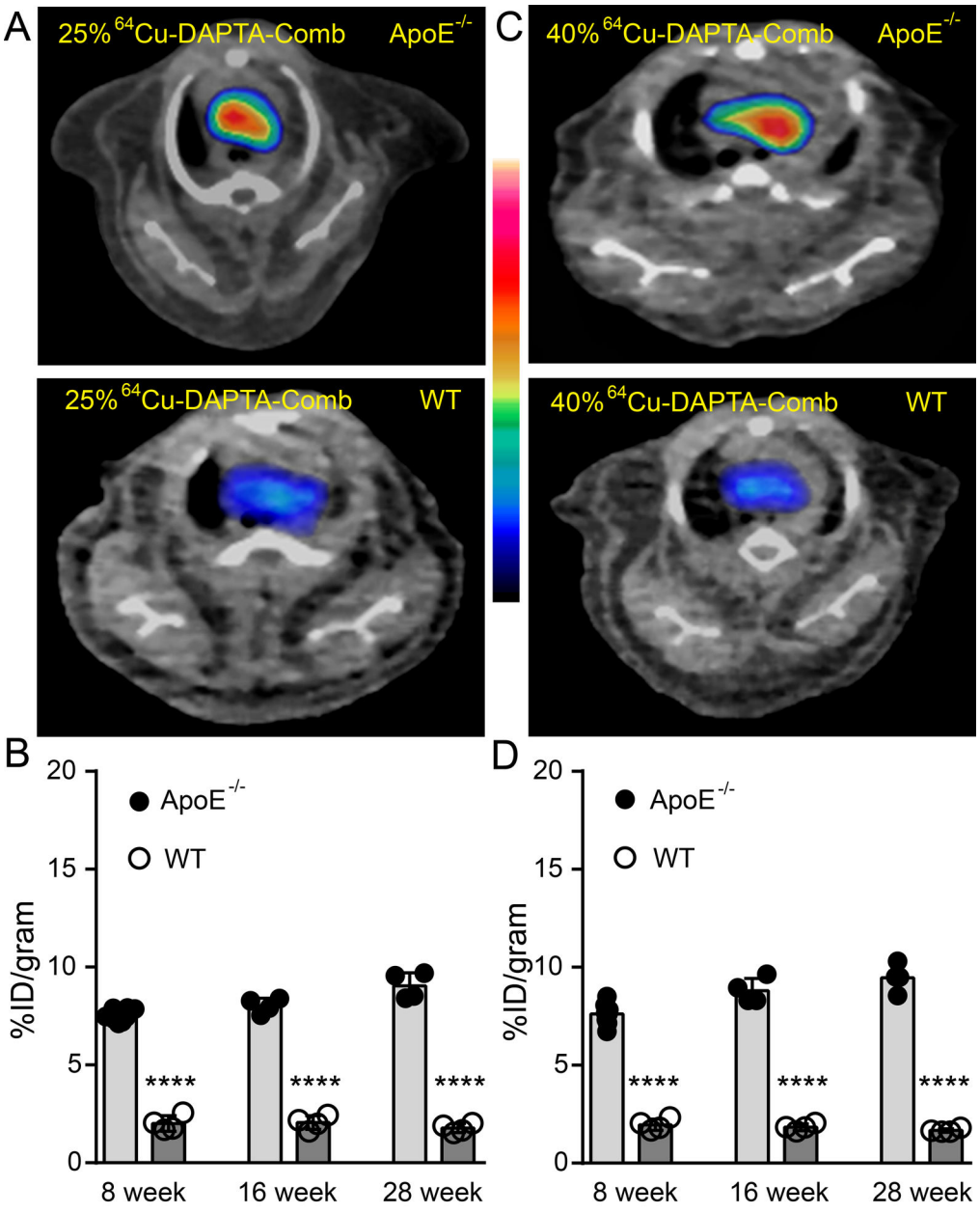

Figure 3.

(A) PET/CT images of 25% and 40% ^{64}Cu-DAPTA-Comb in ApoE$^{-/-}$ mice at 28 weeks post HFD. Images acquired at 24 h post injection showed intensive PET signals at aortic arches compared to the low accumulation in WT mice on normal chow (B) Quantitative uptake analysis of 25% and 40% ^{64}Cu-DAPTA-Comb showed significantly higher uptake in ApoE$^{-/-}$ mice than the age-matched WT C57BL/6 mice along the progression of atherosclerosis from 8 weeks to 28 weeks on HFD (****, $p<0.0001$, n=4–6/group).

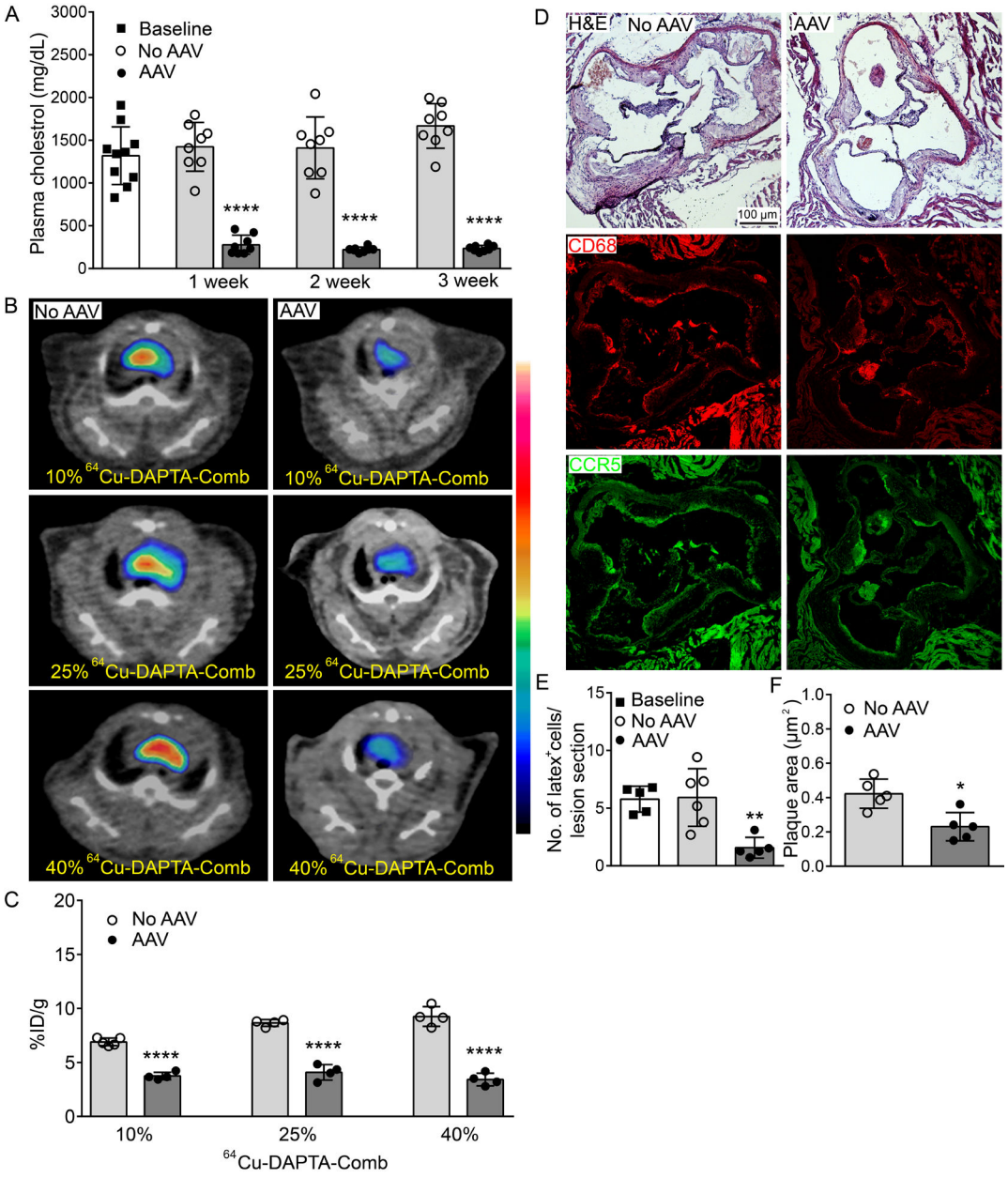

Figure 4.

(A) Measurement of plasma cholesterol levels in ApoE$^{-/-}$ mice at 9 weeks post HFD (baseline) and 1, 2, and 3 weeks post AAV treatment. The non-treated (No AAV) ApoE$^{-/-}$ mice were also measured at the same time points. (B) PET/CT images of 10%, 25%, and 40% ^{64}Cu-DAPTA-Comb showed strong PET signals in the untreated group and weak uptake in AAV treated ApoE$^{-/-}$ mice (n=4/group). (C) Quantification of tracer uptake of the three nanoparticles at 3 weeks post treatment showed significantly decreased uptake in AAV group compared to the untreated group. (D) Comparison of H&E, CD68 (red), and CCR5 (green) immunostaining between AAV and no AAV mice. H&E showed decrease lipid pool, less neointimal thickening, and reduced foam cells on plaques. Immunostaining showed less CD68 and CCR5 in the AAV treated ApoE$^{-/-}$ mice. (E) Counting of latex+ cells at baseline,

No AAV and AAV groups. Decreased signals in the AAV group confirmed the reduced recruitment of monocytes (n=4/group). (F) Quantification of plaque area between AAV and no AAV groups (n=4/group). *p<0.05, ** p<0.01, **** p<0.0001.

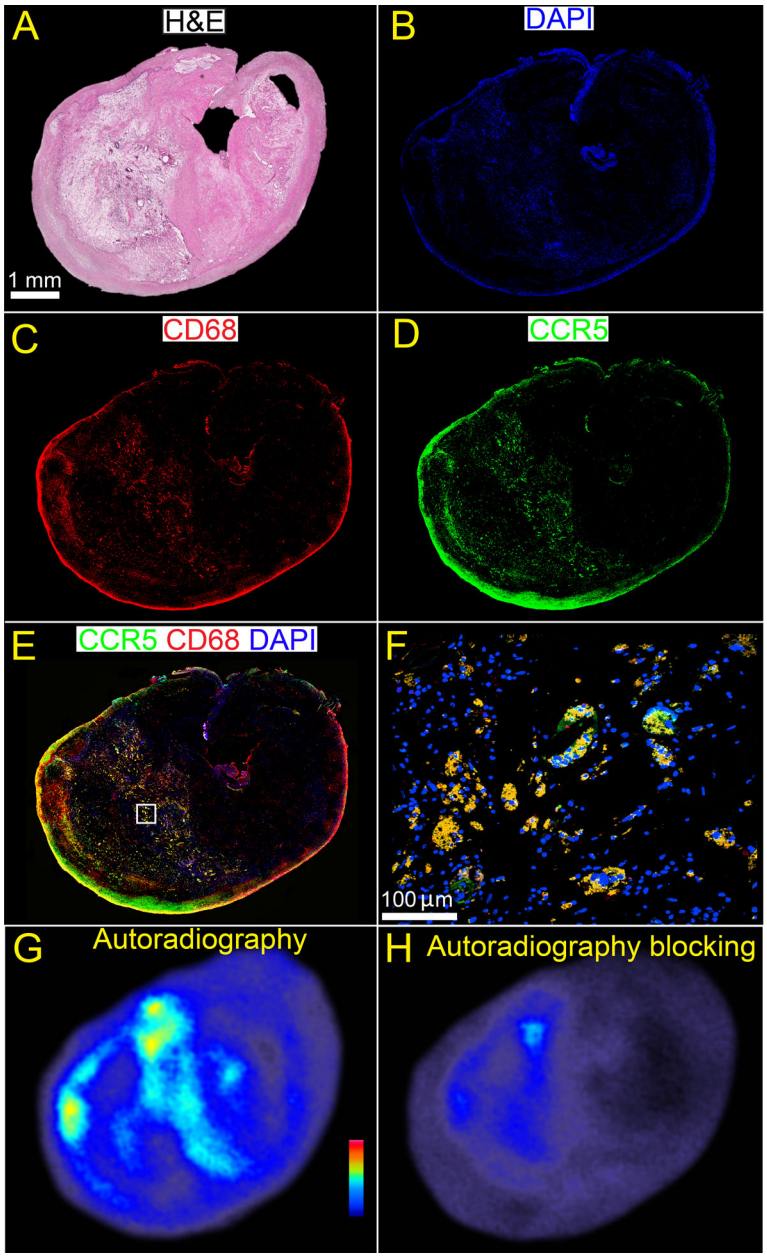

Figure 5.

Ex vivo characterization of human CEA specimen. (A) H&E showed large lipid pool, necrotic core, significant neointimal thickening, and regions with thin fibrous cap. Immunofluorescent staining of (B) DAPI (blue), (C) CD68 (red), and (D) CCR5 (green) showed over-expression of CD68+ macrophages and CCR5 in the necrotic core. DAPI, CD68, and CCR5 fused (E) and amplified (F) immunofluorescent images showed that most CCR5 signals co-localized (yellow) with CD68 macrophages. (G) Representative autoradiography of 40% ^{64}Cu-DAPTA-Comb binding to CEA specimen *ex vivo* showing similar profile to CCR5 signals in (D). (H) Competitive *ex vivo* autoradiography blocking of

40% ^{64}Cu-DAPTA-Comb using 100× non-radioactive 40% DAPTA-Comb. Note: (A) H&E was from Reference 33 due to the use of same human CEA specimen.

Table 1

Characterization of non-targeted Comb and 10%, 25%, and 40% DAPTA-Comb

Polymer	M_n [a]	Đ [a]	Hydro dynamic Size (nm) [b]	ζ-potential (mV)	# of DAPTA/ nanoparticle [c]	# of DOTA/ nanoparticle [c]	^{64}Cu radiolabeling specificity activity (GBq/nmol)
Comb	220,000	1.2	20.0	−32.0	0	105	5.1
10% DAPTA-Comb	200,000	1.7	14.8	−6.24	14	105	4.5
25% DAPTA-Comb	300,000	2.5	15.2	−10.0	35	105	3.8
40% DAPTA-Comb	358,000	2.9	10.9	−14.7	56	105	4.6

[a] Determined by gel permeation chromatography in dimethylformamide, calibrated to poly(methyl methacrylate) standards (g/mol), $Đ = M_W/M_n$.

[b] Measured by dynamic light scattering.

[c] Predicted incorporation.